Vehicular Communications 44 (2023) 100677

Contents lists available at ScienceDirect

Vehicular Communications

journal homepage: www.elsevier.com/locate/vehcom

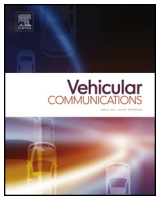

Cellular localizability of unmanned aerial vehicles ☆

Irshad A. Meer *, Mustafa Ozger, Cicek Cavdar

School of Electrical Engineering and Computer Science, KTH Royal Institute of Technology, Stockholm, Sweden

ARTICLE INFO

Article history:
Received 27 March 2023
Received in revised form 23 August 2023
Accepted 13 September 2023
Available online 20 September 2023

Keywords:
Localization
Unmanned aerial vehicles
Cellular networks
Interference
Air-to-ground channel

ABSTRACT

To enable pervasive applications of cellular-connected unmanned aerial vehicles (UAVs), localization plays a key role. The successful reception of localization signals from multiple base stations (BSs) is the first step to localize targets, which is called cellular localizability. In this paper, we propose an analytical framework to characterize the B-localizability of UAVs, which is defined as the probability of successfully receiving localization signals above a certain signal-to-interference plus noise ratio (SINR) level from at least B ground BSs. Our framework considers UAV-related system parameters in a three-dimensional environment and provides a comprehensive insight into factors affecting localizability such as distance distributions, path loss, interference, and received SINR. We perform simulation studies to explore the relationship between localizability and the number of participating BSs, SINR requirements of the received localization signals, air-to-ground channel characteristics, and network coordination. We also formulate an optimization problem to maximize localizability and investigate the effects of UAV altitude in different scenarios. Our study reveals that in an urban macro environment, the effectiveness of cellular network-based localization increases with altitude, with localizability reaching 100% above 60 meters. This finding indicates that utilizing cellular networks for UAV localization is a viable option.

1. Introduction

Localization of unmanned aerial vehicles (UAVs) is a critical component to enable safe and efficient operation in diverse application scenarios such as urban air mobility (UAM) [2–4]. Accurate localization data empowers UAV operators to optimize flight paths, avert collisions, and facilitate timely search and rescue missions [5,6].

Automatic Dependent Surveillance-Broadcast (ADS-B) technology, relying on the Global Positioning System (GPS) [6] is a notable means of localizing aerial vehicles, such as airplanes. Nonetheless, for UAVs, exclusive reliance on GPS raises safety concerns, particularly in scenarios involving beyond visual line of sight (LoS) operations. The susceptibility of GPS to issues like erratic performance in urban landscapes and GPS spoofing from diverse sources [7–9] exacerbates concerns. These challenges necessitate exploration into alternative localization strategies.

A promising solution is cellular network-based localization, which presents several advantages. Firstly, unlike ground users, UAVs encounter LoS channel conditions from multiple neighboring base stations (BSs) [10], rendering them suitable for range-based localization. Secondly, the integration of UAVs into cellular networks permits location data sharing, fostering secure and safe operations [11]. Lastly, the widespread coverage of cellular networks enables UAV localization without requiring additional hardware deployment.

Cellular network-based localization is a part of range-based methods, generally involving two stages [12]. The first stage entails the successful reception of multiple localization signals (reference signals) by a receiver to obtain location-related information. The second stage employs these measurements to estimate the agent node's location through the estimation algorithm at the receiver. The selection of the estimation algorithm will depend on the employed localization techniques, such as received signal strength (RSS), time of arrival (TOA), time difference of arrival (TDOA), or angle of arrival (AOA) [12].

Regardless of the chosen localization technique, the efficacy of localization hinges on three critical factors [13,14]: (i) the target's spatial relationship with nearby BSs, (ii) the number of participating BSs, and (iii) the precision of the selected location estimation algorithm. While most literature emphasizes the third factor to enhance estimation precision [15,16], it assumes uninterrupted reception of location reference signals from a number of sources. This assumption becomes less applicable, particularly for UAVs, due to probabilistic air-to-ground (A2G) channel conditions. To deepen our understanding of the opportunity and limitations imposed by

☆ A preliminary version of this paper has been presented in IEEE WCNC 2020 [1].

* Corresponding author.
E-mail addresses: iameer@kth.se (I.A. Meer), ozger@kth.se (M. Ozger), cavdar@kth.se (C. Cavdar).

https://doi.org/10.1016/j.vehcom.2023.100677

A2G links on the successful reception of the localization signals, we introduce the metric *cellular localizability*. This metric signifies the probability that a UAV receives detectable localization signals from a specific number of ground BSs [13,1]. Detectable signals are those where the signal-to-interference plus noise ratio (SINR) is greater than a threshold. Furthermore, the number of required signals depends on the localization method used in estimating the location of the target. For example, localization methods implementing TDOA-based techniques require signals from at least four BSs for the location estimation of the target device.

It is worth mentioning that, unlike conventional metrics such as the Cramer Rao Lower Bound (CRLB) that set a lower boundary for error variance related to accuracy, localizability emphasizes successful signal reception probability. Consequently, localizability is not directly concerned with the accuracy of localization. The performance in terms of the error bound given by CRLB does not consider the non-deterministic conditions such as network coverage, traffic load, and channel condition. Instead, it only considers a deterministic network with perfect channel conditions for the general analysis of all possible variations.

In most of the existing literature, the problem of the localization of a generic 3D target with range-based techniques has been studied in the context of improving the estimation algorithms with favorable channel conditions. The authors in [17], [18], and [19] under the assumption of LoS channel conditions have developed 3D location estimators for RSS and AOA range-based techniques. These works are not directly applicable to the UAVs as they assume to receive the required strong decodable signals for the estimation.

Y. Li et al. in [20] consider cellular networks for RSS-based localization of the UAVs to calculate the CRLB. They assume a generic LoS channel model and do not consider localizability before calculating the estimation bounds. In literature, consideration of cellular localizability is limited to terrestrial targets only. J. Schloemann et al. in [13] investigate cellular localizability for terrestrial user devices with the help of stochastic geometry. They also show how obtaining a higher number of participating BSs enhances localization precision performance. However, their approach assumes an infinite number of randomly distributed BSs across an unbounded area, an impractical assumption. In [21], the authors adopt narrowband Internet-of-Things (NB-IoT) to study the localizability of the ground sensor nodes. However, they only consider the localization of devices on the ground without considering the challenges of 3D communications. Cellular localizability performance for cellular-connected UAVs is investigated in [1] via simulations by capturing the inherent nature of A2G channels and network dynamics such as interference. However, the statistical characterization of the localizability is missing, which requires a deeper analytical investigation of the path loss, received power, interference, and SINR at the UAV.

In this work, our focus is on providing a comprehensive analysis of cellular localizability for UAVs. Exploring the impact of various factors on cellular localizability like dynamic A2G channel between target UAV and ground BSs. The effect of channel parameters such as path loss exponent which not only depend on the LoS conditions but also on the altitude of the UAV. The importance of the coordination among BSs to limit the interference in the reception of localization signals and localization performance. Additionally, the effect of the network load on the participation of BSs in the localization process.

1.1. Main contribution

In this paper, with the help of the 3GPP channel model [22] for cellular-connected UAVs, we study the localizability performance of the UAVs in terms of different network parameters such as altitude, SINR threshold, and network load. Our main contributions are summarized as follows as compared to the most related works [1,13,21]:

- We propose an analytical framework to analyze UAV localizability. Our interest is the downlink communication-based localization for cellular-connected UAVs. The impact of UAV altitude, the number of participating BSs, and network coordination on the localizability performance are studied in detail. We investigate the effect of the environment for three different scenarios, which are urban micro (UMi), urban macro (UMa), and rural macro (RMa) scenarios.
- Based on the system model, we derive the cumulative distribution functions (CDFs) and probability density functions (PDFs) of the path loss, interference, and received SINR at the target UAV. It includes undertaking the A2G channel characteristics into consideration such as the effect of the UAV altitude on LoS and NLoS channel conditions.
- We provide the approximated analytical results and compare them with simulation results for localizability. Simulation results for different scenarios are also provided.
- An optimization problem is formulated to find the altitude that maximizes the localizability. We performed approximations to solve the problem and obtain localizability performance.
- We provide insights toward the design parameters such as processing gain requirements and network coordination to enhance the signal strength for the localizability of UAVs.

The paper is organized as follows. Section 2 explains our system model. Section 3 provides a theoretical analysis of the localizability and optimization problem formulation for maximizing the localizability with respect to the altitude of UAVs. Section 4 presents performance results of the localizability for different network parameters and channel conditions. Finally, Section 5 concludes our paper.

2. System model

We model the network as a two-tier cellular network with hexagonal tessellation for analytical tractability, which is a common assumption for 5G and beyond networks [23]. The two-layer hexagonal tessellation comprises 19 BSs (denoted as $T = 19$), the UAV to be localized (also referred to as target UAV) is assumed to be within the boundaries of the center cell at an altitude denoted by h_{UT}, depicted in Fig. 1. The dashed brown arrows shown in Fig. 1 represent the localization signals received by the target UAV from the BSs participating in the localization process. Distance relations between the UAV and one of the participating BSs are shown with the black solid arrows in Fig. 1. Key notations to explain the system model are provided in Table 1.

We consider the downlink positioning, which involves the transmission of localization signals from the BSs to the UAV [24]. We also assume universal frequency reuse on the localization signals. The adjacent BSs share control information with each other via the high-speed backhaul links e.g., X2 interface shown in Fig. 1. The X2 links enable synchronization and coordination among the BSs [25]. We consider the three 3GPP-defined scenarios for the UAVs [22]; UMi-AV (urban micro with aerial vehicles), UMa-AV (urban macro with aerial vehicles), and RMa-AV (rural macro with aerial vehicles).

For any localization method to work, the target UAV must receive localization signals from multiple sources with an SINR value greater than a specific threshold. The number of sources and the threshold depend on the localization method implemented. For example, in the timing based localization, the estimated time difference translates into circles around the BS, and the intersection

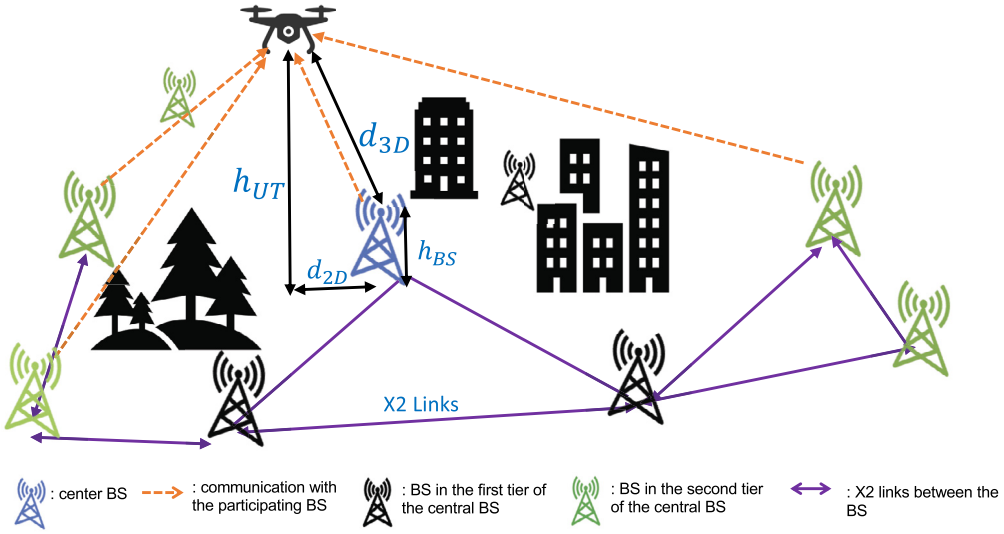

Fig. 1. System model for cellular localizability, localization signals and distance relations.

Table 1
Key notations used.

Notation	Description
h_{UT}, h_{BS}	Altitude of the UAV, base station height
d_i	3D distance between the UAV and i-th participating BS
d_k	3D distance between the UAV and k-th non-participating BS
P_t	Transmitted power from the BS
ζ	Independent shadowing effect
σ^2	Variance of the additive white Gaussian noise
PL_m	Path loss between BS and the UAV, $m \in \{LoS, NLoS\}$
T	Total number of BSs in the network
$\mathcal{T}$	Set of BSs in the network
B	Number of BSs taking part in the localization of the UAVs
f_c	Carrier frequency used
$\mathcal{I}_1$	Interference from BSs participating in localization
$\mathcal{I}_2$	Interference from BSs not taking part in localization
$\mathcal{I}$	Total cumulative interference to the localization of the UAV
α	SINR threshold before the processing gain
β	SINR threshold after the processing gain
γ	Processing gain required
p	Activity factor modeling the coordination among the B participating BSs
q	Activity factor modeling the network traffic load from $(T-B)$ non participating BSs
r_k	Indicator variable, equal to one with probability p, and equal to zero with the probability $(1-p)$, for the k-th BSs
s_j	Indicator variable, equal to one with probability q, and equal to zero with the probability $(1-q)$, for the j-th BSs
P^z	Probability of LoS ($z = LoS$) and NLoS ($z = NLoS$)
P_B	Probability that B BSs have SINR greater than threshold

of these circles provides the location of the target UAV. For better accuracy, more BSs should participate in the multilateration procedure. The minimum required number of participating BSs changes for different methods. For instance, in the case of AOA and TDOA, the minimum requirements for the number of participating BSs are two and four, respectively [26].

Under the same modulation and coding scheme, interference from the other BSs acts as one of the major hindrances in obtaining localization signals from the required number of participating BSs. Thus, making the SINR as the most suitable metric to capture the effectiveness of any localization signal. Furthermore, after the UAVs have processed the localization signals, they transmit their location information with payload data. We make the assumption of seamless synchronization among the participating BSs. This synchronization is attained through packet-based time alignment, commonly implemented using the Precision Time Protocol (PTP), which is specified as IEEE 1588 [27].

2.1. Channel model

In this paper, we adopt the 3GPP channel model proposed in [22] for cellular-connected UAVs flying below 120 m. The channel model depends on the probability of LoS, P^{LoS}, which is defined as below:

$$P^{LoS} = \begin{cases} 1, & d_{2D} \le d^1 \\ \frac{d^1}{d_{2D}} + \exp\left(\frac{-d_{2D}}{p_1}\right)\left(1 - \frac{d^1}{d_{2D}}\right), & d_{2D} > d^1 \end{cases}, \quad (1)$$

where d_{2D} is the distance between the BS and the UAV projected on the ground plane, h_{UT} is the altitude of the UAV as seen in Fig. 1. h_{UT} can be greater or smaller than the height of the BS, h_{BS}. The parameters p_1 and d^1 for three scenarios are given in Table 2.

The path loss PL_m, where $m \in \{\text{LoS}, \text{NLoS}\}$ for the LoS and NLoS link conditions, respectively, are calculated as follows [22]:

$$PL_{LoS} = 28.0 + 22\log_{10}(d_{3D}) + 20\log_{10}(f_c), \quad (2)$$

Table 2
3GPP channel model parameters [22].

Scenario	p_1	d^1
UMi-AV	$233.98\log_{10}(h_{UT}) - 0.95$	$\max(294.05\log_{10}(h_{UT}) - 432.94, 18)$
UMa-AV	$4300\log_{10}(h_{UT}) - 3800$	$\max(460\log_{10}(h_{UT}) - 700, 18)$
RMa-AV	$\max(15021\log_{10}(h_{UT}) - 16053, 1000)$	$\max(1350.8\log_{10}(h_{UT}) - 1602, 18)$

$$PL_{NLoS} = -17.5 + (46 - 7\log_{10}(h_{UT}))\log_{10}(d_{3D}) + 20\log_{10}(\frac{40\pi f_c}{3}), \quad (3)$$

where d_{3D} is the 3D distance between the BS and the UAV, and f_c is the carrier frequency in GHz.

We incorporate shadowing effects, where signal variations are modeled by a Gaussian distributed random variable ζ with a standard deviation that varies with height [22], described as $4.64\exp(-0.0066h_{UT})$ (for LoS), 6 dB (NLoS). However, the effects of small-scale fading are neglected, as they tend to be smoothed out when considering the average signal strength. This average incorporates broader temporal factors like path loss and shadowing and is consistent with the current models for evaluating cellular localization performance [28,29].

2.2. Antenna gain

In our system model, we consider a single omnidirectional antenna with unitary gain for the UAV. For the ground BSs, we assume a vertical N-element uniform linear array (ULA), where each element is omnidirectional in azimuth with a maximum gain of g_E^{max}. Directivity as a function of the zenith angle (ϕ) is given by the following [30]:

$$g_E(\phi) = g_E^{max}\sin^2(\phi), \quad (4)$$

where ϕ is the zenith angle between the ground BS and the UAV. Considering half-wavelength spacing between the adjacent antenna elements and a fixed down-tilt angle ϕ_t, the array factor of the ULA is calculated as

$$g_A(\phi) = \frac{\sin^2(N\pi(\cos\phi - \cos\phi_t)/2)}{N\sin^2(\pi(\cos\phi - \cos\phi_t)/2)}. \quad (5)$$

The overall antenna gain of BSs in linear scale is calculated as

$$g(\phi) = g_E(\phi) \times g_A(\phi). \quad (6)$$

2.3. SINR calculation

Based on the above channel models, the received SINR at the UAV at altitude (h_{UT}) from an ith ($i \in \mathcal{T}$) BS, which is at a 3D distance of $d_{3D} = d_i$ is calculated as

$$SINR_i = \frac{P_r(h_{UT}, d_i)}{\mathcal{I} + \sigma^2}, \quad (7)$$

where $P_r(h_{UT}, d_i)$ is the received power and is given as

$$P_r(h_{UT}, d_i) = P_t g_i(\phi)\zeta_i PL_m^{-1}(h_{UT}, d_i), \quad (8)$$

where P_t is the transmitted power from the ith BS to the UAV and is assumed to be same for all the BSs, $g_i(\phi)$ is the antenna gain, ζ_i denotes the independent shadowing affecting the signal strength. The cumulative interference from the concurrently transmitting BSs excluding the ith BS is denoted by $\mathcal{I}$ and is calculated as

$$\mathcal{I} = \sum_{k\in\mathcal{T} \text{ and } k\neq i} P_t g_k(\phi)\zeta_k PL_m^{-1}(h_{UT}, d_k), \quad (9)$$

where d_k is the 3D distance between the UAV and the kth BS ($k \in \mathcal{T}$ and $k \neq i$), which are transmitting at the same time. Among the $|\mathcal{T}| = T$ BSs, B number of BSs ($B \leq T$) with the strongest time average received signal strength participate in the localization process. However, their participation is successful only if they have SINR greater than a given threshold.

A processing gain γ is considered to enhance the localizability signal strength by integrating the incoming signals in time. Therefore, we have two SINR definitions at the receiver: pre-processing SINR, which is the SINR before any processing gain, and post-processing SINR after applying the gain. The pre-processing SINR provided in (7) is given without the gain providing an improvement on the localization signal strength to meet the requirements.

It is also important to note here that the 5G opens new dimensions to improve the localization performance thanks to New Radio (NR) framework [29]. It proposes new capabilities such as downlink positioning reference signal (PRS) with different numerology and frequency options such as frequencies below 6 GHz and above 24 GHz. BSs can utilize different PRS sequences to reduce mutual interference. These sequences can follow different comb structures that use certain subcarriers in designated symbols [31].

In case of the UAV, as the altitude increases, the probability of LoS condition with ground BSs increases resulting in better reception of useful signals from the intended BS. However, it also leads to a higher level of interference from the unintended BSs. To avoid interference, the B participating BSs attempt to coordinate and avoid allocating the same radio resources. However, perfect coordination among all B BSs is not always possible. As a result, they simultaneously transmit their localization signals on the same radio resources with a probability p. The parameter p encapsulates the effectiveness of X2 link performance in facilitating coordination among the participating BSs. A value of $p = 0$ indicates perfect coordination achieved through X2 links, resulting in no interference, while $p = 1$ signifies the absence of coordination via X2 links. Meanwhile, due to network load, each of the remaining $(T - B)$ BSs may also transmit simultaneously using the same radio resources with probability q. To account for coordination among the participating BSs and the traffic demands in the non-participating BSs, we introduce two independent random variables: r_k for the participating BSs and s_j for the non-participating BSs. To capture participating and non-participating BSs in our analysis, the SINR calculated in (7) can be reformulated as:

$$SINR_i(B) = \frac{P_t g_i(\phi)\zeta_i PL_m^{-1}(h_{UT}, d_i)}{\mathcal{I}_1 + \mathcal{I}_2 + \sigma^2}, \quad (10)$$

where $\mathcal{I}_1$ represents the cumulative interference from the participating BSs and $\mathcal{I}_2$ represents the cumulative interference from the non-participating BSs. Their mathematical definitions are given as follows:

$$\begin{aligned}\mathcal{I}_1 &= \sum_{k=1 \text{ and } k\neq i}^{B} r_k P_r(h_{UT}, d_k) \\ &= \sum_{k=1 \text{ and } k\neq i}^{B} r_k P_t g_k(\phi)\zeta_k PL_m^{-1}(h_{UT}, d_k),\end{aligned} \quad (11)$$

$$\mathcal{I}_2 = \begin{cases} \sum_{j=1+B}^{T} s_j P_r(h_{UT}, d_j) = \sum_{j=1+B}^{T} s_j P_t g_j(\phi) \zeta_j P L_m^{-1}(h_{UT}, d_j), \\ \quad \text{if B < T} \\ 0, \quad \text{if B = T}, \end{cases} \tag{12}$$

where r_k and s_j follow Bernoulli distribution. r_k and s_j being equal to one with probability p and q, respectively, and equal to zero with the probability $(1-p)$ and $(1-q)$, respectively. The activity parameters associated with participating and non-participating BSs make the $SINR_i$ in (10) as a function of B.

3. Theoretical analysis of localizability performance

In this section, we develop a theoretical framework to analyze the localizability performance of a target UAV with the help of cellular networks. We first derive the B-localizability as the function of the received SINR and the number of participating BS B. The received SINR dependents on the received power, cumulative interference and noise. To obtain the distribution of the received power, we need to calculate the distribution of the distances and path loss involved. These steps are provided in the sequel.

3.1. Base stations participating in the localization

Let us define a random variable Ψ as the maximum number of BSs successfully participating in the localization process. Given our system model, the definition of Ψ is given as follows:

$$\Psi = \underset{B \in \mathcal{T} \text{ and } B \leq T}{\arg\max} \; B \times \prod_{i=1}^{B} \mathbb{1}\left(SINR_i(B) \geq \alpha\right), \tag{13}$$

where B is the number of BSs participating in the localization and having the strongest signal at the UAV, and SINR is given as in (10). $\mathbb{1}(\theta)$ is the indicator function which is equal to 1 if θ is true and equal to 0 if θ is false. Hence, Ψ will be equal to B when all the signals from the B BSs have an SINR value greater than the threshold.

We define B-localizability as the probability that at least B BSs successfully participate in the localization procedure [13]. B-localizability, P_B, is defined as:

$$P_B = Pr(\Psi \geq B) = 1 - F_\Psi(B), \tag{14}$$

where $F_\Psi(B)$ is the CDF of Ψ and is defined as:

$$\begin{aligned} F_\Psi(B) &= Pr(\Psi < B) = 1 - Pr(\Psi \geq B) \\ &= 1 - Pr\left(\left(\prod_{i=1}^{B} \mathbb{1}\left(SINR_i(B) \geq \alpha\right)\right) = 1\right). \end{aligned} \tag{15}$$

The B-localizability metric can also be viewed as a coverage metric that quantifies the probability of receiving decodable localization signals from B BSs at the receiver. For instance, in the case of the TDOA localization scheme that requires at least four decodable signals ($B = 4$) for unambiguous localization, P_4 represents the probability of achieving this criterion. A value of $P_4 = 0.99$ indicates that the target UAV may receive at least four decodable signals with a probability of 99%.

The distribution of B-localizability in (15) depends on SINR distribution at the target UAV from participating BSs. Hence, we statistically characterize each component to calculate SINR defined in (10) in the following subsections.

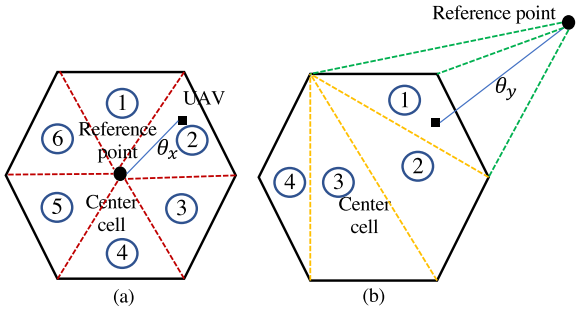

Fig. 2. The random 2D distance between the UAV and the reference BSs, where the UAV is distributed randomly in the center cell. (a) θ_x is the 2D distance between a random point of the UAV within a cell and the BS at the center cell. (b) θ_y is the 2D distance between a random point of the UAV within a cell and the BS at a neighboring cell.

3.2. 2D distance and altitude distribution

The received power and interference at the target UAV are influenced by the distance between the BSs and the UAV. Therefore, to determine the SINR distribution at the target UAV, we first need to calculate the distance distribution between the BSs and the UAV's projection point on the ground (i.e., 2D distance). Since the target UAV is located randomly in the central hexagon cell, it will have two random 2D distances associated with it, which will depend on the point of reference used for their calculation. Specifically, the first random distance is the distance between the random location of the target UAV and the central BS (or the center of the hexagon as the reference point), denoted as θ_x in Fig. 2(a). The second random distance is the distance between the random location of the target UAV in the central hexagon cell and any of the neighboring BS (used as the reference point), denoted as θ_y in Fig. 2(b). Therefore, the first step is to determine the distributions of these two random distances: 1) the distance (θ_x) from a reference point inside the hexagon to a random point within the hexagon, and 2) the distance (θ_y) from a reference point outside the hexagon to a random point inside the hexagon.

Let $F_{\theta_x}(r)$ and $F_{\theta_y}(r)$ represent the CDF of θ_x and θ_y, respectively. To obtain the distribution of the random distances θ_x and θ_y, we adopt an approach similar to that presented in [32]. This approach involves the use of decomposition and recursion techniques to calculate the distance distribution in a polygon. Specifically, we use the known distance distributions from a vertex of an arbitrary triangle to a random point inside, to compute the distribution of random distances from an arbitrary reference point (inside or outside) to any polygon.

To implement this approach, we first triangulate (i.e., divide into triangles) the hexagonal cell with respect to the reference points. For calculating $F_{\theta_x}(r)$, the reference point is inside and at the center of the central hexagonal cell. Thus, we triangulate the cell into six triangles with respect to the center, as depicted in Fig. 2(a). Similarly, for calculating $F_{\theta_y}(r)$, the reference point is outside of the central hexagonal cell. Hence, we triangulate the cell into four non-overlapping triangles with respect to one of the vertexes of the hexagon, as shown in Fig. 2(b).

Overall, this triangulation and decomposition approach allows us to obtain the distance distribution for a given reference point and polygon. Once we know the distribution of distances within each triangle, we can use probabilistic summation to compute the final distance distribution. Specifically, the CDF of the distance distributions $F_{\theta_x}(r)$ will be given by a probabilistic sum of the CDF of the distance distribution in each of the six triangles. Let $F_\theta^K(r)$ represent the CDF of the distance distribution from a vertex to a randomly chosen point within a given triangle (κ), such as trian-

gle ② illustrated in Fig. 2(a). To ascertain the distance distribution from the vertex to a randomly selected point within the triangle (κ), we initiate the process by drawing a circle centered at the said vertex. In this setup, the radius of the circle, denoted as θ_x, corresponds directly to the distance between the vertex and the random point situated within the triangle (κ). The probability that this distance measures less than θ_x, essentially the CDF (F_θ^κ), is equal to the area of the intersection between the circle and triangle (κ) divided by total area of the triangle (κ), denoted as $\mathcal{A}_\kappa$ [32]. Subsequently, the CDF $F_{\theta_x}(r)$ for the distance distribution from the center to a randomly selected point within the polygon can be determined through probabilistic summation, given as:

$$F_{\theta_x}(r) = \sum_{\kappa=1}^{\Omega} \frac{\mathcal{A}_\kappa}{\mathcal{A}} F_\theta^\kappa(r), \tag{16}$$

where Ω is the number of triangles formed in the polygon with BS as the reference. $\mathcal{A}_\kappa$ is the area of the κth triangle, where $\mathcal{A}$ is the area of the cell. In the case of the hexagon where the triangulation takes place at the center, Ω is equal to six, which is seen in Fig. 2(a).

The CDF of the distance distribution F_{θ_y} is similar to $F_{\theta_x}(r)$ given in (16), but with one key difference: $F_\theta^\kappa(r)$ is the CDF of the distance distribution from a point outside of the triangle to a random point located in the κth triangle (e.g., triangle ① in Fig. 2(b)), which is provided in [32]. In Fig. 2(b), the reference point (in this case, the BS) is situated outside the center cell, the cell gets divided into four triangles with respect to one of its vertex. The CDF of the distance distribution F_{θ_y} will be given as the probabilistic summation of distance distributions for all four triangles in the central cell as in (16).

The other distance distribution for UAVs is for the altitude of the UAV. We assume a uniform distribution with a CDF of $F_H(h)$ within the limits between 20 m and 120 m.

3.3. Statistical characterization of path loss and received power

Characterization of the path loss as the CDF at a certain altitude of h_{UT} is provided in the following due to its dependence on LoS probability:

$$F_{PL}(d) = \sum_{z\in\{LoS,NLoS\}} P^z F_{PL,z}(d), \tag{17}$$

where $F_{PL,LoS}(d)$ and $F_{PL,NLoS}(d)$ are derived as follows:

$$\begin{aligned} F_{PL,LoS}(d) &= Pr(PL_{LoS}(d_{3D}) \le d) \\ &= Pr\left(\eta_{LoS}\left(\sqrt{d_{2D}^2 + h_{UT}^2}\right)^{a_{LoS}} \le d\right) \\ &= Pr\left(d_{2D} \le \sqrt{(d/\eta_{LoS})^{2/a_{LoS}} - h_{UT}^2}\right) \\ &= \sum_{\kappa=1}^{\Omega} \frac{\theta_\kappa}{\theta} F_\theta^\kappa\left(\sqrt{(d/\eta_{LoS})^{2/a_{LoS}} - h_{UT}^2}\right), \end{aligned} \tag{18}$$

where we model the path loss for the LoS condition in (2) as $PL_{LoS} = \eta_{LoS} d_{3D}^{a_{LoS}}$, η is the attenuation constant and a is the path loss exponent. Similarly, in case of the NLoS, the distribution for the path loss can be calculated as:

$$F_{PL,NLoS}(d) = \sum_{\kappa=1}^{\Omega} \frac{\theta_\kappa}{\theta} F_\theta^\kappa\left(\sqrt{(d/\eta_{NLoS})^{2/a_{NLoS}} - h_{UT}^2}\right), \tag{19}$$

Let R be the received signal strength at the UAV from a BS which can be described as the difference between the transmitted power (P_t) and the path loss (PL). Then, the CDF $F_R(r)$ of the received power is calculated as:

$$\begin{aligned} F_R(r) = Pr(R \le r) &= Pr((P_t - PL) \le r), \\ &= Pr((P_t - r) \le PL), \\ F_R(r) &= 1 - F_{PL}(P_t - r). \end{aligned} \tag{20}$$

The PDF $f_R(r)$ of the received power is $f_R(r) = F_R'(r)$

3.4. Statistical characterization of interference

As provided in (10), the interference to the UAV is due to both participating BSs ($\mathcal{I}_1$) and non-participating BSs ($\mathcal{I}_2$). Both interference components, $r_k P_r(h_{UT}, d_k)$ and $s_j P_r(h_{UT}, d_j)$ given in (11) and (12) respectively, are products of independent binary variables and the continuous received signal strength random variable. The independent binary variables are used to model the cooperation with the participating BSs and the traffic load in non-participating BSs. Let χ denote the discrete binary random variable r_k or s_j depending on the BS to be either participating or non-participating one, and R denote the continuous received signal strength random variable ($F_R(r)$ is already defined in (20)). Hence, to represent interference to the UAV from a single kth ($k \in [1, B]$) participating BS, we define a new random variable $I_{1,k} = \chi R$. The CDF of the $I_{1,k}$ will be then as follows:

$$\begin{aligned} F_{I_{1,k}}(i) = Pr(\chi R \le i) &= Pr(\chi = 1) Pr(\chi R \le i \mid \chi = 1) \\ &\quad + Pr(\chi = 0) Pr(\chi R \le i \mid \chi = 0), \\ &= \begin{cases} p F_R(i) + (1-p), & \text{if } i > 0, \\ (1-p), & \text{if } i = 0, \end{cases} \end{aligned} \tag{21}$$

where $F_R(i)$ is defined in (20), p is the probability r_k being equal to 1. $F_{I_{1,k}}(i)$ provides the distribution of interference at the UAV from a single participating BS. For the distribution of the interference from a jth ($j \in [B+1, T]$) non-participating BS, $F_{I_{2,j}}$, is derived in same way as in (21) with final expression as:

$$F_{I_{2,j}}(i) = \begin{cases} q F_R(i) + (1-q), & \text{if } i > 0, \\ (1-q), & \text{if } i = 0, \end{cases} \tag{22}$$

Under given conditions, we can consider the interference from the BSs as independent. $F_{I_{1,k}}(i)$ and $F_{I_{2,j}}(i)$ show the individual interference distribution from a single random BS.

The cumulative distribution of the overall interference at the receiver is obtained by the convolution of the individual interference distributions as follows:

$$F_I(i) = F_{I_{1,1}}(i) \circledast \ldots F_{I_{1,B}}(i) \circledast F_{I_{2,B+1}}(i) \circledast \ldots F_{I_{2,T}}(i), \tag{23}$$

where $\circledast$ is the convolution operator. The PDF $f_I(i)$ of the cumulative interference is the calculated as $f_I(i) = F_I'(i)$.

3.5. Statistical characterization of SINR

The received SINR defined in (7) is a function of the received power and the cumulative interference. For simplicity of notation, we denote the SINR by S, the received power by R, and the cumulative interference by I. The probability distribution of the received SINR can be derived using the probability distributions of the received power $f_R(r)$ and cumulative interference $f_I(i)$. For tractability, we consider the received power and the cumulative interference to be bounded between a minimum and a maximum value, i.e., $R \in [r_{min}, r_{max}]$, and $I \in [i_{min}, i_{max}]$.

Given the value of any two out of the three parameters, S, R, and I, the value of the third parameter can be calculated using (7). Let the SINR corresponding to received power R and cumulative interference I be denoted by $g_S(R, I)$. The received power corresponding to the SINR value S and cumulative interference I is denoted by $g_R(I, S)$ and cumulative interference corresponding to SINR value S and received power R is denoted by $g_I(R, S)$.

Assuming that the received power R and the cumulative interference I are independent, the largest value of the SINR would be achieved when the received power is maximum and the interference is minimum and is given as $g_S(r_{max}, i_{min})$. The lowest value of the SINR is achieved when the received power is minimum and the interference is maximum and is given as $g_S(r_{min}, i_{max})$. Therefore, we can obtain the CDF of the SINR at the UAV by considering $g_S(r_{min}, i_{max}) \leq S \leq g_S(r_{max}, i_{min})$. This is calculated as follows:

$$Pr(S \leq \alpha) = \begin{cases} \int_{g_I(\alpha, r_{min})}^{i_{max}} \int_{r_{min}}^{g_R(\alpha, i)} f_R(r) f_I(i) d_r d_i, \\ \quad if\ g_S(r_{min}, i_{max}) \leq \alpha \leq g_S(r_{min}, i_{min}); \\ \int_{i_{min}}^{i_{max}} \int_{r_{min}}^{g_R(\alpha, i)} f_R(r) f_I(i) d_r d_i, \\ \quad if\ g_S(r_{min}, i_{min}) \leq \alpha \leq g_S(r_{max}, i_{max}); \\ 1 - \int_{i_{min}}^{g_I(\alpha, i_{max})} \int_{g_R(\alpha, i)}^{r_{max}} f_R(r) f_I(i) d_r d_i, \\ \quad if\ g_S(r_{max}, i_{max}) \leq \alpha \leq g_S(r_{max}, i_{min}); \end{cases} \tag{24}$$

Since it is also possible to have $g_S(r_{max}, i_{max}) < g_S(r_{min}, i_{min})$, the CDF of the SINR can also be written as follows:

$$Pr(S \leq \alpha) = \begin{cases} \int_{g_I(\alpha, r_{min})}^{i_{max}} \int_{r_{min}}^{g_R(\alpha, i)} f_R(r) f_I(i) d_r d_i, \\ \quad if\ g_S(r_{min}, i_{max}) \leq \alpha \leq g_S(r_{max}, i_{max}); \\ \int_{i_{min}}^{i_{max}} \int_{r_{min}}^{g_R(\alpha, i)} f_R(r) f_I(i) d_r d_i, \\ \quad if\ g_S(r_{max}, i_{max}) \leq \alpha \leq g_S(r_{min}, i_{min}); \\ 1 - \int_{i_{min}}^{g_I(\alpha, i_{max})} \int_{g_R(\alpha, i)}^{r_{max}} f_R(r) f_I(i) d_r d_i, \\ \quad if\ g_S(r_{min}, i_{min}) \leq \alpha \leq g_S(r_{max}, i_{min}). \end{cases} \tag{25}$$

3.6. Operational altitudes for maximum localizability

Based on the previous discussion, it is evident that the localizability performance is directly linked to the received SINR at the UAV. Additionally, due to the impact of the UAV altitude on both the channel gain and the antenna gain, the received SINR at the UAV is a non-linear function of the altitude. Therefore, our objective is to determine the relationship between the localizability performance in terms of (P_B) and the UAV altitude. We can achieve this by formulating an optimization problem that seeks to identify the altitude that maximizes the localizability performance (P_B) as follows:

$$\max_{h_{UT}} \sum_{i \in \mathcal{T}} \mathbb{1}(SINR_i \geq \alpha) \tag{26}$$

subject to:

(**C1**) $h_{UT} \leq h_{\max}$,

(**C2**) $h_{UT} \geq h_{\min}$,

where **(C1)** stands for the maximum allowed altitude for the UAV, and **(C2)** assures that a UAV is moving in the air above a certain altitude as per [22]. The objective function in (26) maximizes the number of BSs with SINR greater than the threshold α with respect to the altitude of the UAV. The objective function in our case depends on the distribution of the SINR at the UAV given in Section 3.5. Since the distribution does not have a closed-form expression, it is difficult to solve this optimization problem with conventional optimization methods. Therefore, we use a discrete brute force approach with Monte-Carlo simulations for obtaining the dependence of localizability probability on the altitude of the UAV. This approach is explained as follows.

We assume that there are UAVs distributed randomly in a plane in the center cell at discrete altitudes. We seek to maximize the numbers of UAVs which receive an SINR greater than some threshold from at least B number of BSs with respect to the altitude of the UAV. Thus, we find the optimal altitude that maximizes the localizability of UAVs. Let j denote the location in the center cell where the UAV is located, h $(h_{min} \leq h \leq h_{max})$ denotes the UAV altitude and i $(i \in \mathcal{T})$ denotes considered BS. Next, we present our optimization problem whose goal is to determine the altitude of each UAV which maximizes the localizability by the network as follows:

$$\arg\max_{h_{min} \leq h_{UT} \leq h_{max}} (\varphi_h), \tag{27}$$

$$\varphi_h = \sum_j b_{j,h},\ \forall h \tag{28}$$

$$b_{j,h} = 1, \text{if} \sum_i a_{i,j,h} \geq B,\ \forall j, h; \tag{29}$$

$$a_{i,j,h} = 1, \text{if}\ (SINR_{i,j,h} \geq \alpha),\ \forall i, j, h; \tag{30}$$

where $SINR_{i,j,h}$ is the received SINR at UAV j at altitude h from BS i. $a_{i,j,h} = 1$ in (30) means the SINR from the BSs i to the UAV j at altitude h is above a certain threshold α, $b_{j,h} = 1$ in (29) means that total number of BSs having SINR greater than the threshold (α) is at-least B. The φ_h in (28) means the number of the location at which the SINR constraint is satisfied for B number of BSs at different altitudes. The objective function in (27) gives us the UAV altitude h_{UT} which maximizes the total number of locations at which the SINR from at least B BSs is greater than the threshold.

Note that there is no guarantee that limited samples of the UAVs in (30) capture the distribution of the SINRs. In order to solve this problem, we used our analytical calculation and compare the simulation results obtained using the approach in (28)-(30) as shown in Fig. 3. Since the simulation results and the analytical results are overlapping, it shows that our approach captures the analytical evaluation.

Table 3
Parameters for numerical study.

Parameters	UMi-AV	UMi-AV	UMi-AV
Inter-site distances	200 m	500 m	1732 m
BSs antenna height	10 m	25 m	35 m
Carrier frequency	2 GHz	2 GHz	800 MHz
Bandwidth (B_w)	10 MHz		
Noise figure (NF)	9 dB		
Transmit power	46 dB m		
Maximum element gain (g_E^{max})	8 dBi		
Number of elements (N)	8		
Down-tilt angle (ϕ_t)	102°		
Variance	$4.64\exp(-0.0066h_{UT})$ (for LoS), 6 dB(NLoS)		
Noise Power [dB m]	$10\log_{10}(400 \cdot 10^{-20}) + NF + 10\log_{10}(B_w)$ [33]		

4. Simulation results and discussion

We use Monte Carlo simulation and the snapshot model to analyze the localizability in Matlab. In our simulations, we performed 100,000 iterations with the target UAV randomly located in the center cell to obtain the localizability probability. We adopt the 3GPP channel model for the UAVs [22] in three different scenarios: UMi-AV, UMa-AV, and RMa-AV. The simulation parameters are given in Table 3.

4.1. B-localizability performance

In the case of 3D mobility of cellular-connected UAVs, it is hard to obtain an exact SINR distribution due to its dependency on air-to-ground channel characteristics with LoS conditions and changing shadowing variance with the UAV's altitude, and cooperation between participating and non-participating BSs. The SINR distribution provided in Section 3.5 is computationally intensive. Hence, to provide the analytical results, we use an approximate method. We use (16) to get the distance distribution of the UAV in the central cell of the network. The received power and the interference are obtained from (20)-(23), for different locations in the central cell. Hence, to have approximate results for the analytical derivations that we present in Section 3, we use empirical CDFs for resulting SINRs. According to these CDFs, we calculate P_B when $B = 4$, i.e., if the fourth highest SINR value is greater than the threshold pre-processing SINR, α, as we outline in (14) and (15). For fixed $p = 1$, $q = 1$ and $B = 4$, we obtain the analytical and simulation results for P_B in an urban micro scenario in Fig. 3. In the worst case with no coordination, i.e., $p = 1$, $q = 1$, both participating and non-participating BSs in the network interfere in the localization process. In Fig. 3, P_4 is almost one in simulation results at SINR thresholds below -12 dB. This is because a very low threshold constraint at the UAV is achieved easily by the localization signals even in worst-case scenarios with lower received power for the localization signals. We also observe that P_4 becomes almost zero for the SINR threshold greater than 0 dB. This means that without any gain or interference cancellation, it is difficult to achieve the required localizability performance. Since the analytical and the simulation results coincide, our result will depend on the empirical SINR values obtained by our extensive simulations in the following sections.

4.2. B-localizability performance with different number of participating BSs

In order to analyze B-localizability with a change in the number of participating BSs, we assume a pre-processing SINR threshold of -6 dB [14]. We analyze all the three scenarios to observe the B-localizability for different B values at different altitudes in Fig. 4. We observe in the case of the UMi scenario, a B-localizability becomes 0.4 when $h_{UT} = 60$ m and all BSs act as interferers,

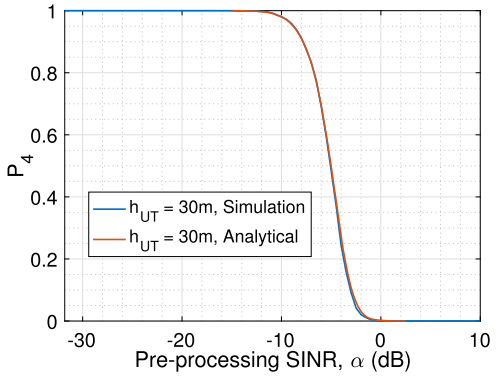

Fig. 3. P_4 vs. pre-processing SINR threshold α when $p = 1$, $q = 1$ for urban micro scenarios.

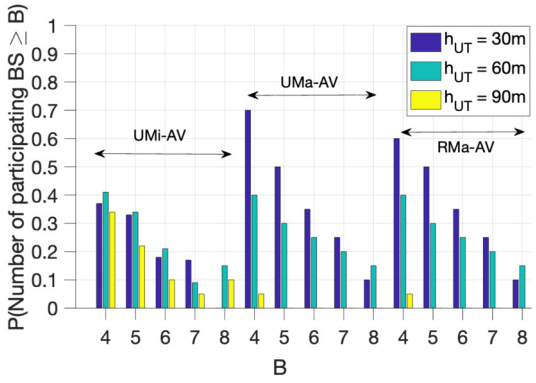

Fig. 4. P_B vs. number of participating BSs, B, when $p = 1$, $q = 1$ for three different scenarios.

i.e., $p = 1$, $q = 1$. In general, as we increase the altitude h_{UT}, B-localizability decreases except for certain altitudes like around $h_{UT} = 60$ m for the UMi scenario where localizability increases. This is because of the antenna radiation pattern at the BS which favor certain altitudes. On the other hand, as altitude increases, the higher path loss experienced in the channels becomes dominant, and the localizability performance decreases. The same effect is observed for the urban macro and rural scenarios. As we move from the urban to the rural scenario, the LoS probability increases due to fewer obstacles in the rural area and we observe an increase in the localizability performance. Another interesting observation is that in the case of the UMi scenario, as the number of participating BSs, B, increases, the B-localizability decreases and tends to be zero when $B = 8$ for $h_{UT} = 30$ m. Thus, it becomes impossible to implement a localization method where the required number of participating BSs are eight or more. In the case of the UMa and RMa scenarios, we see that the B-localizability for $h_{UT} = 60$ m and $B = 8$ is higher than in the case of the UMi. Hence with an

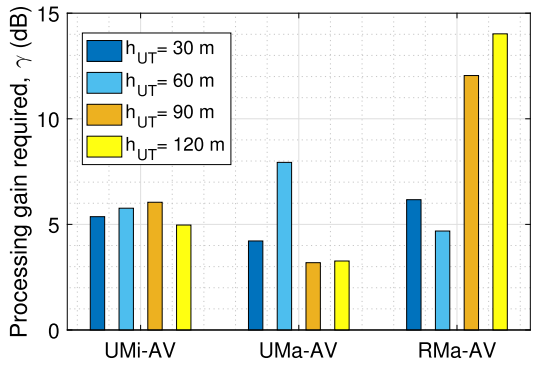

Fig. 5. Processing gain required for achieving $P_4 = 0.9$ for different altitudes, h_{UT}, when $p = 1$, $q = 1$ for three different scenarios.

interference mitigation technique, it is possible to implement localization methods that require a higher number of participating BSs.

4.3. Processing gain requirement with the number of participating BSs

In order to gain some insight into design parameters such as the processing gain at the target UAV, it is important to observe the change in the gain with respect to the altitude of the UAV. A sufficient gain provided to the received localization signals can achieve an acceptable P_B. For achieving $P_4 = 0.9$ with an SINR threshold of -6 dB, Fig. 5 shows the variation of the gain requirements for different altitudes. We observe that the gain requirement does not follow a trend with the altitude of the UAV. This is because of the antenna gain achieved as a function of the antenna tilt in (4) which makes some altitudes favorable for the localization. Fig. 5 shows the same analysis for the UMa and RMa scenarios.

We observe that variation in the required gain is small for the urban environment as compared to the rural. Since the wireless channel has almost the same path loss but a different probability of NLoS link conditions in urban areas, the variation in the gain is small. Dynamic allocation of gain with altitude at the receiver can improve localization performance. Based on the altitude and the localization method, the UAV can select the gain to achieve the successful participation of the required number of BSs.

4.4. UAV altitude for maximum localizability performance

As explained in Section 3.6, we obtain the dependence of the localizability probability for $B = 4$ on the altitude of the UAV and observe how some of the altitudes are more favorable for localization in different scenarios. In Fig. 6, we observe the B-localizability for $B = 4$ as a function of UAV altitude h_{UT} for different coordination levels in three different scenarios. In Fig. 6(a), we consider the urban micro scenario, Fig. 6(b), urban macro scenario, and Fig. 6(c), the rural scenario with all the non participating BSs interfering ($q = 1$), while we change the coordination among the participating BSs. We observe for all the scenarios with perfect coordination has the best performance in terms of localizability. For the urban scenarios in 6(a), the localizability first increases as the UAV moves up and then decreases before increasing again. This is because of the small inter-site distance and the antenna pattern at the BSs. Therefore, we have certain altitudes where the localizability performance is highest as in Fig. 6(a) for $h_{UT} = 40$ m; Fig. 6(b) for $h_{UT} = 90$ m; and Fig. 6(c) for $h_{UT} = 50$ m. In the rural scenario, we observe that there is an improvement in the localizability performance and maximum localizability is achieved around $h_{UT} = 50$ for the cases with partial coordination. As the altitude increases, localizability performance decreases for all the coordination (p) values. This is because path loss due to the distance plays a major role as compared to the antenna beam gain.

Fig. 7 shows the B-localizability for $B = 4$ as a function of UAV altitude h_{UT} for different pre-processing SINRs (α). We consider the case where we have full coordination among the participating BSs for different pre-processing SINR requirements. We observe that even with perfect coordination, we do not have the best localizability performance at all altitudes. We observe for the urban scenario in Fig. 7(a), the performance peaks at around $h_{UT} = 40$ m, showing that the tilt in the BS antennas and the resulting radiation pattern make the altitude range around $h_{UT} = 40$ m favorable for the maximum localizability. For the urban macro scenario in Fig. 7(b), we observe a very low localizability probability value at around $h_{UT} = 40 - 50$ m. However, as altitude increases beyond $h_{UT} = 50$ m, localizability experiences a notable improvement, peaking at approximately $h_{UT} = 65$ m. Notably, altitudes exceeding $h_{UT} = 60$ meters exhibit an increased potential for favorable localizability. This is because of the reduction in the density of obstacles at higher altitudes within the urban macro scenario, facilitating LoS A2G links with multiple BSs. In this scenario, the dense distribution of BSs, coupled with perfect coordination, leads to reduced interference from neighboring BSs. Consequently, SINR improves, resulting in enhanced localizability performance. Also, the antenna gain compensates for the inherent path loss that arises due to increased distance. In the rural scenario in Fig. 7(c), we do not see the effect of the antenna pattern on the localizability performance because of the large inter-site distances in rural areas where the signal strength is almost the same over the range of the altitudes. The results of Fig. 6 and Fig. 7 provide us with insights for obtaining maximum localizability results just by changing the operational altitude of the UAV in different scenarios.

4.5. Network coordination and network traffic

To illustrate the impact of interference mitigation through network coordination among the B participating BSs, we change the parameter p to vary the level of coordination. This captures the coordination among the participating BSs while non-participating BSs are transmitting, i.e., $q = 1$. In Fig. 8a, considering the UMi scenario with $B = 4$ and a predefined pre-processing SINR threshold, the plot demonstrates an ascending trend in P_4 as the level of coordination (p) intensifies. Heightened coordination, where one BS transmits while others remain idle or transmit on other channels, leads to elevated B-localizability. The enhancement in B-localizability showcases the potential of mitigating interference from neighboring BSs through efficient network coordination.

We explore the impact of traffic among the non-participating BSs by changing q. This parameter encapsulates varying traffic intensities. Setting the parameter q to 1 implies that non-participating BSs are catering to users on the same channel, including other UAVs. This introduces additional interference from these BSs. While $q = 0$ represents perfect coordination among the non-participating BS, resulting in no interference with the target UAV. In Fig. 8b, for the same UMi scenario with $B = 4$, an ascending trend in P_4 is observed as traffic among non-participating BSs decreases. However, the impact of the traffic on localizability is comparatively less substantial than that achieved through network coordination. This result arises from the fact that participating BSs, being in closer proximity with the UAV to be localized, exert a more pronounced impact on SINR compared to non-participating BSs situated at greater distances. Consequently, the effect of non-participating BSs serving more users in the downlink on SINR and localizability is relatively small.

Additionally, we assess the B-localizability performance with $B = 4$ for a UAV in a UMi scenario, as it moves beyond the cellular network's coverage area i.e., away from all the BSs in the

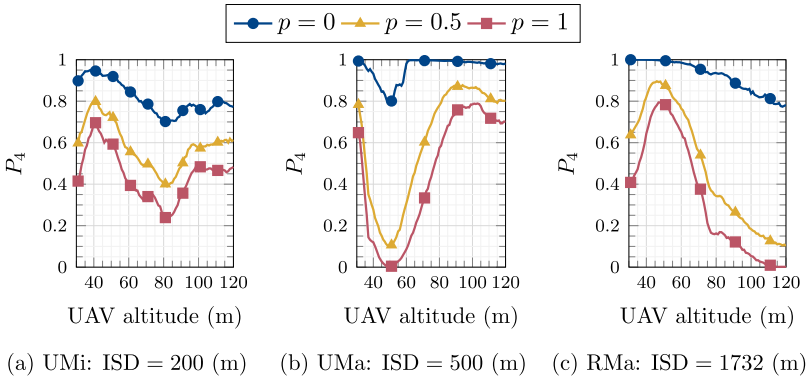

Fig. 6. Localizability probability P_4 vs. UAV altitude h_{UT} (m), for different coordination level p, with $q = 0$.

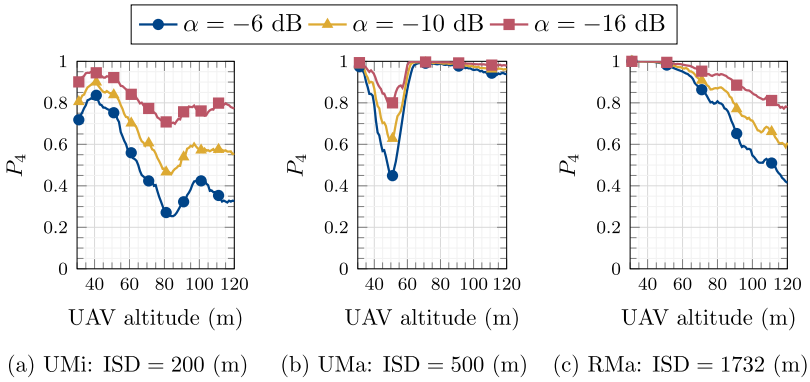

Fig. 7. Localizability probability P_4 vs. UAV altitude h_{UT} (m), for different pre-processing SINR (α), with perfect coordination ($q = 0$, $p = 0$).

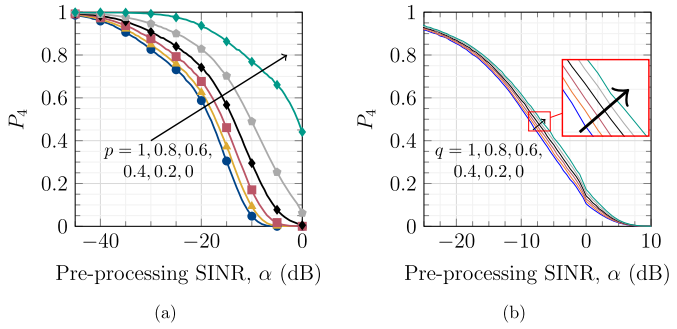

Fig. 8. P_4 vs. pre-processing SINR threshold, α when $h_{UT} = 30$ m, (a) $q = 1$, and p varying from 1 to 0 with a step of 0.2; (a) $p = 1$, and q varying from 1 to 0 with a step of 0.2.

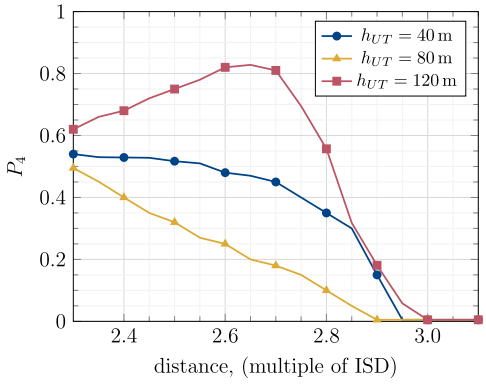

Fig. 9. P_4 vs. communication distance from the central BS going away from the coverage region of the two-tier cellular network.

two-tier network. The performance results for P_4 are illustrated in Fig. 9, depicting its variation with the distance from the central BS, where the BSs have coverage till the distance equal to 2.5 times the ISD. These results are obtained under specific system parameters, including a pre-processing SINR threshold of $\alpha = -16$ dB, $p = 1$, $q = 1$, and $h_{UT} = 40, 80, 120$ m and an ISD = 200 m. At altitudes of 40 m and 80 m for the UAV, P_4 drops to zero as the UAV moves farther away. This is expected since at lower heights, the UAV faces NLoS channels from both nearby and distant BSs. As the distance grows, the signal quality diminishes, resulting in a decrease in SINR. Comparing $h_{UT} = 40$ m to $h_{UT} = 80$ m, we find better localizability at the lower altitude, supporting our initial finding that for the UMi scenario, localizability performance at $h_{UT} = 80$ m is very low. At $h_{UT} = 120$ m, an interesting trend emerges: with increasing distance, localizability improves notably. This happens because, at higher altitudes, the UAV usually has a LoS link with most BSs. While moving away, the interference from distant BSs decreases, while the nearest BSs maintain strong signal strength due to a clear LoS channel and full power transmission. This interference reduction boosts the SINR, enhancing localizability.

4.6. BS deployment model and communication frequency

We revisit our assumption that base stations (BSs) are distributed based on a hexagonal grid model. Our objective is to illustrate how this assumption aligns with the localizability outcomes produced by the Poisson Point Process model to show the generalizability of our approach. Fig. 10a effectively contrasts the localizability outcomes obtained through these random and hexagonal deployment scenarios. This comparison is conducted across varying numbers of participating BSs while maintaining the BS density and constant parameters such as $\alpha = -16$ dB, $h_{UT} = 40$

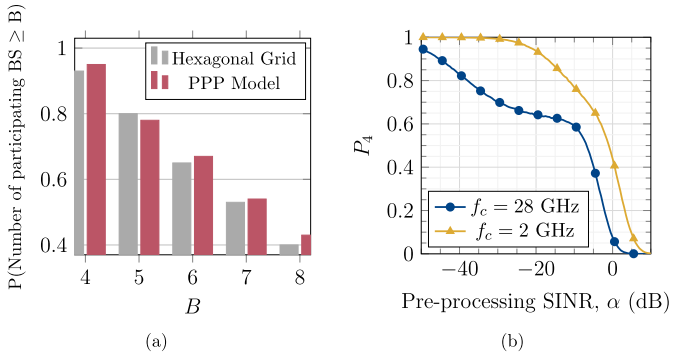

Fig. 10. Localizability results for an urban micro scenario (a) BS distribution comparison, (b) Frequency range impact.

m, and $p = q = 0$. The variance of shadowing within our channel model is substantial enough to observe a convergence between the hexagonal grid model and the Poisson distribution of BSs. This alignment leads to the convergence of results from both models.

In Fig. 10b, we compare the localizability under different frequency ranges for $B = 4$. The two frequency ranges being compared are $f_c = 2$ GHz, and $f_c = 28$ GHz. The results for the $f_c = 28$ GHz frequency range are obtained using the channel model provided in [34]. With the perfect coordination in an urban micro scenario, i.e., $p = 0$, $q = 0$, both participating and non-participating BSs in the network do not interfere in the localization process. In Fig. 10b, P_4 shows a difference for the two frequency ranges as the signal at $f_c = 28$ GHz is more susceptible to various losses due to NLoS channel, path loss, and atmospheric absorption. Therefore, the localizability performance is the worst at higher frequency ranges. Nonetheless, a notable advantage stemming from this analysis is that it suggests the possibility of utilizing lower frequency ranges for precise localization while reserving higher frequency ranges for more efficient data transmission purposes.

4.7. Model application: insights and limitations

Insights: This localizability analysis represents the initial step towards enabling UAV localization within cellular networks. The localizability metric serves as a valuable tool for designers to measure the ability of the network to localize UAVs and help in selecting optimal localization techniques based on environment, BS deployment, and UAV altitudes. Our findings demonstrate that enhancing localizability performance is achievable through techniques such as processing gain, inter-BS coordination, and strategically operating UAVs within altitude ranges conducive to favorable localizability outcomes across diverse scenarios. For example, we can gain valuable insights into the ability of a network, utilizing a localization technique reliant on a minimum of four localization signals, to accurately locate a UAV flying at an altitude of 80 meters. For such a case in rural settings with sparsely distributed BSs, its localizability surpasses 80%, indicating effective localization is possible. However, at the same altitude in a densely deployed urban micro scenario, the localizability drops to less than 30%, illustrating challenges in accurate UAV localization with the given method.

Limitations: Our study does not take into account a specific interference avoidance model to accommodate interference coordination schemes. We simplify the control process of interference by coordination through a single parameter. For more specific interference coordination methods, this parameter needs to be updated. However, this simplification effectively captures the influence of interference, albeit without encompassing the precise methods of interference coordination. Also, in our present model, we employ a snapshot approach to calculate localizability. However, there is potential for enhancing the tracking of a moving UAV's position by incorporating its time series location data. Exploring how correlations within the sequential location data can be leveraged to boost localizability performance is a promising avenue for improvement.

5. Conclusion

In this paper, we analyze the B-localizability of cellular-connected unmanned aerial vehicles (UAVs), which is the probability of successfully receiving localization signals from at least B participating base stations (BSs) with a signal to interference plus noise ratio (SINR) above a certain threshold. We base our investigation on the scenarios outlined by 3GPP for cellular-connected UAVs. To calculate localizability, we propose an analytical framework that considers both UAV-specific parameters and network-related parameters. We use Monte-Carlo simulations to study the effects of altitude, the number of participating BSs, and coordination among them on the localizability. We also analyze the processing gain requirement for achieving the required localizability performance. We formulate an optimization problem to maximize localizability and find the best operational altitudes in different scenarios. Our findings suggest that the ideal altitude range for cellular localization is not the same for all BS deployments. While urban micro scenario with densely deployed BSs and perfect coordination show the best localizability performance between 30 and 60 meters, urban macro environments have the optimal performance above 60 meters. Similarly, the rural scenario with sparsely deployed BS and perfect coordination show appreciable localizability performance at all altitudes. Future work should include practical tests to investigate the effects of network and UAV-specific parameters as well as UAV mobility on the localizability performance.

Declaration of competing interest

The authors declare that they have no known competing financial interests or personal relationships that could have appeared to influence the work reported in this paper.

Data availability

No data was used for the research described in the article.

Acknowledgements

This work was supported in part by the CELTIC-NEXT Project, 6G for Connected Sky (6G-SKY), with funding received from Vinnova, Swedish Innovation Agency.

References

[1] I.A. Meer, M. Ozger, C. Cavdar, On the localization of unmanned aerial vehicles with cellular networks, in: Proc. IEEE WCNC, 2020, pp. 1–6.
[2] A. Menichino, V. Di Vito, B. Dziugiel, A. Liberacki, H. Hesselink, M. Giannuzzi, Urban air mobility perspectives over mid-term time horizon: main enabling technologies readiness review, in: 2022 Integrated Communication, Navigation and Surveillance Conference (ICNS), IEEE, 2022, pp. 1–13.
[3] A. Baltaci, E. Dinc, M. Ozger, A. Alabbasi, C. Cavdar, D. Schupke, A survey of wireless networks for future aerial communications (FACOM), IEEE Commun. Surv. Tutor. 23 (4) (2021) 2833–2884.
[4] M. Ozger, M. Vondra, C. Cavdar, Towards beyond visual line of sight piloting of UAVs with ultra reliable low latency communication, in: 2018 IEEE Global Communications Conference (GLOBECOM), IEEE, 2018, pp. 1–6.
[5] R. Shrestha, R. Bajracharya, S. Kim, 6g enabled unmanned aerial vehicle traffic management: a perspective, IEEE Access 9 (2021) 91119–91136.
[6] I.A. Meer, M. Ozger, M. Lundmark, K.W. Sung, C. Cavdar, Ground based sense and avoid system for air traffic management, in: Proc. IEEE PIMRC, 2019, pp. 1–6.
[7] B. Hofmann-Wellenhof, H. Lichtenegger, J. Collins, Global Positioning System: Theory and Practice, Springer Science & Business Media, 2012.

[8] A Survey on Radio Frequency Based Precise Localisation Technology for UAV in GPS-Denied Environment, J. Intell. Robot. Syst. 103 (3) (2021) 1–30.
[9] E. Wallischeck, GPS Vulnerabilities in the Transportation Sector, US Department of Commerce, Washington, DC, USA, 2016.
[10] A. Azari, F. Ghavimi, M. Ozger, R. Jantti, C. Cavdar, Machine learning assisted handover and resource management for cellular connected drones, in: 2020 IEEE 91st Vehicular Technology Conference (VTC2020-Spring), IEEE, 2020, pp. 1–7.
[11] X. Lin, V. Yajnanarayana, S.D. Muruganathan, S. Gao, H. Asplund, H.-L. Maattanen, M. Bergstrom, S. Euler, Y.-P.E. Wang, The sky is not the limit: LTE for unmanned aerial vehicles, IEEE Commun. Mag. 56 (4) (2018) 204–210.
[12] J.A. del Peral-Rosado, et al., Survey of cellular mobile radio localization methods: from 1G to 5G, IEEE Commun. Surv. Tutor. 20 (2) (2018) 1124–1148 (Second Qtr. 2018).
[13] J. Schloemann, H.S. Dhillon, R.M. Buehrer, Toward a tractable analysis of localization fundamentals in cellular networks, IEEE Trans. Wirel. Commun. 15 (3) (2015) 1768–1782.
[14] J. Schloemann, H.S. Dhillon, R.M. Buehrer, Localization performance in cellular networks, in: Proc. IEEE International Conference on Communication Workshop (ICCW), 2015, pp. 871–876.
[15] T. Wang, H. Xiong, H. Ding, L. Zheng, TDOA-based joint synchronization and localization algorithm for asynchronous wireless sensor networks, IEEE Trans. Commun. 68 (5) (2020) 3107–3124.
[16] K. Shamaei, Z.M. Kassas, Receiver design and time of arrival estimation for opportunistic localization with 5g signals, IEEE Trans. Wirel. Commun. 20 (7) (2021) 4716–4731, https://doi.org/10.1109/TWC.2021.3061985.
[17] S. Chang, Y. Zheng, P. An, J. Bao, J. Li, 3-d rss-aoa based target localization method in wireless sensor networks using convex relaxation, IEEE Access 8 (2020) 106901–106909.
[18] Q. Wang, Z. Duan, X.R. Li, Three-dimensional location estimation using biased rss measurements, IEEE Trans. Aerosp. Electron. Syst. 56 (6) (2020) 4673–4688.
[19] S. Tomic, M. Beko, R. Dinis, 3-d target localization in wireless sensor networks using rss and aoa measurements, IEEE Trans. Veh. Technol. 66 (4) (2016) 3197–3210.
[20] Y. Li, F. Shu, B. Shi, X. Cheng, Y. Song, J. Wang, Enhanced rss-based UAV localization via trajectory and multi-base stations, IEEE Commun. Lett. 25 (6) (2021) 1881–1885.
[21] F. Tong, Y. Sun, S. He, On positioning performance for the narrow-band Internet of things: how participating eNBs impact?, IEEE Trans. Ind. Inform. 15 (1) (2018) 423–433.
[22] 3GPP, Study on Enhanced LTE Support for Aerial Vehicles, Tech. rep., 3GPP TR 36.777, 2017.
[23] H. Tabassum, M. Salehi, E. Hossain, Fundamentals of mobility-aware performance characterization of cellular networks: a tutorial, IEEE Commun. Surv. Tutor. 21 (3) (2019) 2288–2308.
[24] C. Laoudias, A. Moreira, S. Kim, S. Lee, L. Wirola, C. Fischione, A survey of enabling technologies for network localization, tracking, and navigation, IEEE Commun. Surv. Tutor. 20 (4) (2018) 3607–3644.
[25] V. Jungnickel, T. Wirth, M. Schellmann, T. Haustein, W. Zirwas, Synchronization of cooperative base stations, in: 2008 IEEE International Symposium on Wireless Communication Systems, IEEE, 2008, pp. 329–334.
[26] S. Hu, A. Berg, X. Li, F. Rusek, Improving the performance of OTDOA based positioning in NB-IoT systems, in: Proc. IEEE Global Communications Conference (GLOBECOM), 2017, pp. 1–7.
[27] J.C. Eidson, M. Fischer, J. White, IEEE-1588™ standard for a precision clock synchronization protocol for networked measurement and control systems, in: Proceedings of the 34th Annual Precise Time and Time Interval Systems and Applications Meeting, 2002, pp. 243–254.
[28] 3GPP, Study on NR positioning support, Tech. rep., 3GPP TR 38.855, 2019.
[29] Chao Yang, Shiwen Mao, Xuyu Wang, An overview of 3GPP positioning standards, GetMobile, Mobile Comput. Commun. 26 (1) (2022) 9–13.
[30] F. Salehi, M. Ozger, N. Neda, C. Cavdar, Ultra-reliable low-latency communication for aerial vehicles via multi-connectivity, in: 2022 Joint European Conference on Networks and Communications & 6G Summit (EuCNC/6G Summit), 2022, pp. 166–171.
[31] C. Yang, S. Mao, X. Wang, An overview of 3GPP positioning standards, ACM GetMobile, Mobile Comput. Commun. 26 (1) (2022) 9–13.
[32] M. Ahmadi, J. Pan, Random distances associated with arbitrary triangles: a recursive approach with an arbitrary reference point, Tech. rep., University of Victoria, 2013.
[33] D. Tse, P. Viswanath, Fundamentals of Wireless Communication, Cambridge University Press, 2005.
[34] P. Wang, M. Ozger, C. Cavdar, M. Petrova, Beyond visual line of sight piloting of UAVs using millimeter-wave cellular networks, in: 2019 IEEE 30th Annual International Symposium on Personal, Indoor and Mobile Radio Communications (PIMRC), IEEE, 2019, pp. 1–7.